Akke S. J. Suiker
Koiter Institute Delft,
Faculty of Aerospace Engineering,
Delft University of Technology,
P.O. Box 5058,
2600 GB Delft, The Netherlands

Norman A. Fleck
Cambridge Center for Micromechanics,
Department of Engineering,
Cambridge University,
Trumpington Street,
Cambridge CB2 1PZ, UK

Frictional Collapse of Granular Assemblies

The frictional collapse of an assembly of equisized spheres is studied by a discrete element model. The macroscopic constitutive response is determined as a function of the level of Coulomb friction between particles. It is found that the level of Coulomb friction has a strong effect upon the relative proportion of sliding and rolling between particles, and consequently upon the macroscopic strength of the granular assembly. The discrete element predictions are shown to be in good agreement with experimental results obtained from triaxial tests on an aggregate of steel spheres. It is demonstrated that the shape of the collapse surface can be adequately represented by the Lade-Duncan continuum model. [DOI: 10.1115/1.1753266]

1 Introduction

Since the pioneering work of Cundall and Strack [1], discrete element models (DEM) have been popular for analyzing the mechanical characteristics of granular materials; see, for example, [2–9]. Most studies focus on two-dimensional particle configurations, where the particles are represented by circular disks. Although two-dimensional discrete element analyses have provided insight into the mechanical response of particle assemblies, they are of limited value in simulating the behavior of advanced laboratory experiments. The response to complicated loading paths, such as those applied to a granular material in a true triaxial apparatus, [10,11], can only be adequately simulated by means of three-dimensional numerical analyses.

Apart from the direct simulation of laboratory tests, three-dimensional discrete element analyses are useful for the development and verification of continuum models of granular compaction and flow. The use of macroscopic stress and strain measures to characterize the deformation state of a granular assembly is valid provided the representative volume element contains a sufficiently large number of particles; under such conditions, the use of average macroscopic variables with a continuum constitutive law leads to major advantages in computational economy compared with the discrete element method.

Various micromechanical models have been derived by homogenisation of microstructural particle interactions, [12–19], although checks on their accuracy by comparison with experiments and with discrete element simulations are lacking. Typically, the micromechanical descriptions are based on upper and lower bounds of the true response. For example, the assumption of ''affine deformation'' gives an approximation for the deformation at the particle contact level in terms of the imposed macroscopic strain field over the particle assembly. This kinematic assumption is often made in the homogenization of granular materials, [12–16,20,21], and commonly results in an overprediction of the macroscopic strength and stiffness, [22–24].

In this paper the discrete element method is used to study the frictional behavior of three-dimensional particle assemblies. The macroscopic constitutive response under axisymmetric stress conditions is determined as a function of the level of Coulomb friction between particles. These predictions are compared to experimental results obtained from triaxial tests on an aggregate of steel spheres. Furthermore, to reveal the degree of local particle rearrangement by sliding and rotation, the assembly of discrete particles is subjected to three different kinematic conditions: (1) both particle sliding and particle rotation are allowed to occur, (2) particle sliding is permitted, but particle rotation is prevented, and (3) particle sliding is allowed to occur in accordance with an affine deformation field, while particle rotation is prevented. Finally, the collapse surface is computed in the deviatoric plane of principal stress space by subjecting the three-dimensional granular assembly to a set of proportional stress paths.

2 Particle Assembly Simulated by Discrete Element Model

The mechanical behavior of a three-dimensional assembly of elastic-frictional particles is studied by employing the discrete element program Particle Flow Code (PFC).[1] In this discrete element program, the system of equations describing the dynamic interaction of an assembly of spherical particles is solved by using an explicit time-stepping scheme; at each time step the change in the interparticle forces is computed from the relative velocities at the particle contacts via the incremental force-displacement relation for each contact. After updating the interparticle forces, the new out-of-balance force at each particle contact is determined and used to calculate the new translational and rotational particle accelerations from Newton's law of motion. Integration of the particle accelerations provides the particle velocities and thereby the particle displacements. The particle displacements give the new particle positions, after which, by using the updated velocities at the particle contacts, the procedure is repeated. Checks are carried out to determine if contacts have become established or have ceased to exist. The normal force versus overlap contact law obeys the well-known Hertzian theory; see, for example, [25]. The contact is either fully sticking (with the tangential stiffness set by the contact area) or undergoes full slip in accordance with the Coulomb friction criterion

$$|f_d^c| \leqslant -f_n^c \tan \phi^c \tag{1}$$

where f_n^c is the normal contact force, f_d^c is the shear contact force, and ϕ^c is the friction angle at the particle contact c. Since the particle contacts are supposed to have no resistance against tension, the normal and shear contact forces are set to zero if the overlap between two particles becomes less than zero. For a more detailed description of the above method, see [1,26].

The geometry used in the computations consists of a cuboidal volume that is randomly filled with spherical particles, see Fig. 1. The particles of the granular assembly are allowed to rotate, un-

Contributed by the Applied Mechanics Division of THE AMERICAN SOCIETY OF MECHANICAL ENGINEERS for publication in the ASME JOURNAL OF APPLIED MECHANICS. Manuscript received by the ASME Applied Mechanics Division, October 22, 2002; final revision, October 9, 2003. Editor: R. M. McMeeking. Discussion on the paper should be addressed to the Editor, Prof. Robert M. McMeeking, Journal of Applied Mechanics, Department of Mechanical and Environmental Engineering, University of California–Santa Barbara, Santa Barbara, CA 93106-5070, and will be accepted until four months after final publication of the paper itself in the ASME JOURNAL OF APPLIED MECHANICS.

[1]Itasca Consulting Group, Inc., Minneapolis, MN, U.S.A.

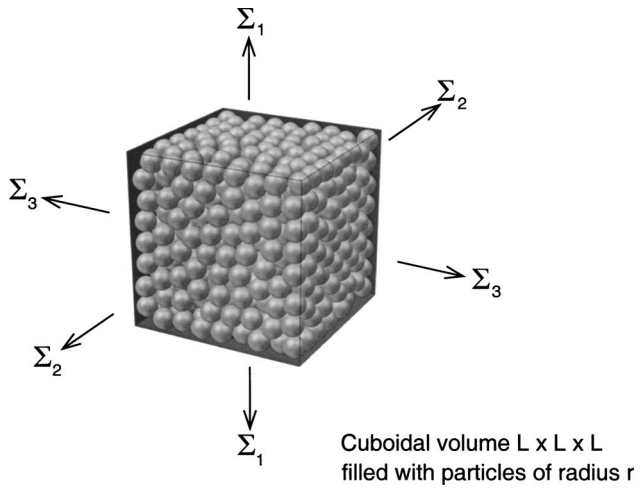

Fig. 1 Cuboidal volume $L\times L\times L$ of equi-sized spheres with radius r, subjected to principal stresses Σ_1, Σ_2, and Σ_3

less otherwise stated. A *strain-controlled* loading path is prescribed by moving the outer walls of the cube towards each other, where the relative wall velocity $\dot{u}_i^{\text{wall}}$ is related to the average macroscopic deformation rate of the assembly, $\dot{E}_{ij}$, by

$$\dot{u}_i^{\text{wall}}=\dot{E}_{ij}L_j \tag{2}$$

with L_j the relative position between points on two opposite faces of the cube. The normal contact stiffness at the walls is chosen to be sufficiently high, such that the walls act as "rigid" objects. The tangential contact stiffness at the walls is set to zero, i.e., the boundary particles may freely slide along the walls.

In order to minimize the inertia forces in a quasi-static analysis, the wall velocity needs to be relatively small. Accordingly, the number of discrete time steps required for reaching a macroscopic deviatoric strain of 5% is specified to lay between 1.0×10^5 and 1.6×10^5. Additional checks have shown that for a selected particle density of 2650 kg/m^3 this number of time-steps leads to negligibly small inertia forces. A *stress-controlled* loading path is prescribed by means of a servo-control algorithm, which adjusts the wall velocities $\dot{u}_i^{\text{wall}}$ to reduce the error between the measured stress Σ_{ij} and the desired stress Σ_{ij}^{des}. This servo-control algorithm has the form

$$\dot{u}_i^{\text{wall}}=g_j(\Sigma_{ij}-\Sigma_{ij}^{\text{des}}) \tag{3}$$

where g_j is the gain, whose appropriate values have been determined by trial and error. The Cauchy stress Σ_{ij} represents the spatial average over a so-called "measurement sphere," and is determined by using the well-known expression [12,17,18,27]

$$\Sigma_{ij}=\frac{1}{2V}\sum_{c=1}^{C}(f_j^c l_i^c+f_i^c l_j^c) \tag{4}$$

where V is the volume of the measurement sphere, C is the total number of particle contacts in the measurement sphere, l_i^c is the branch vector that connects the centers of two neighboring particles in contact, and f_j^c is the contact force at contact "c." The center of the measurement sphere corresponds to the center of the cuboidal volume, and the diameter of the measurement sphere equals the width of the cuboidal volume.

2.1 Convergence Study for Effective Medium Calculation In the discrete element model, a sufficiently large number of particles needs to be determined for mimicking the response of a continuum. This is done by analyzing the response of a cuboidal volume of *equi-sized spherical particles* (often called a "monodisperse packing," [28]), loaded in *axisymmetric compression*, $\Sigma_1<\Sigma_2=\Sigma_3\leqslant 0$. Here, Σ_1, Σ_2, and Σ_3 denote the principal stresses in the longitudinal direction, x_1, and the transverse directions of the specimen, x_2 and x_3, respectively. Stress measures that are commonly employed for describing the mechanical behavior of isotropic particle assemblies are the deviatoric stress (invariant) Σ^{dev} (also known as the "von Mises stress") and the hydrostatic stress (invariant) Σ^{hydr}, given by

$$\Sigma^{\text{dev}}=\sqrt{\frac{3}{2}\Sigma'_{ij}\Sigma'_{ij}}$$
$$\Sigma^{\text{hydr}}=\frac{1}{3}\Sigma_{kk}. \tag{5}$$

Here and below, a repeated suffix denotes summation and Σ'_{ij} is the deviatoric stress tensor according to $\Sigma'_{ij}=\Sigma_{ij}-\Sigma^{\text{hydr}}\delta_{ij}$, with δ_{ij} the well-known Kronecker delta symbol. The stress measures Σ^{dev} and Σ^{hydr} are work conjugates to the deviatoric strain rate $\dot{E}^{\text{dev}}$ and volumetric strain rate $\dot{E}^{\text{vol}}$, respectively, where

$$\dot{E}^{\text{dev}}=\sqrt{\frac{2}{3}\dot{E}'_{ij}\dot{E}'_{ij}}$$
$$\dot{E}^{\text{vol}}=\dot{E}_{kk} \tag{6}$$

and $\dot{E}'_{ij}$ is the deviatoric strain rate tensor given by $\dot{E}'_{ij}=\dot{E}_{ij}-1/3\dot{E}^{\text{vol}}\delta_{ij}$. For an axisymmetric stress configuration, Eq. (5) simplifies to

$$\Sigma^{\text{dev}}=|\Sigma_1-\Sigma_3|$$
$$\Sigma^{\text{hydr}}=\frac{1}{3}(\Sigma_1+2\Sigma_3) \tag{7}$$

and the corresponding strain rates, Eq. (6), simplify to

$$\dot{E}^{\text{dev}}=\frac{2}{3}|\dot{E}_1-\dot{E}_3|$$
$$\dot{E}^{\text{vol}}=\dot{E}_1+2\dot{E}_3 \tag{8}$$

where $\dot{E}_1$ is the longitudinal strain rate, and $\dot{E}_3(=\dot{E}_2)$ is the transverse strain rate.

Two different particle sizes are considered; particles with a radius $r=0.05L$ (cuboidal volume of 1145 particles), and particles with a radius $r=0.025L$ (cuboidal volume of 9167 particles), where L is the length of the sides of the cuboidal volume, see also Fig. 1. After generation of the discrete particle assembly, a confining pressure Σ^{conf} is applied onto the outer walls of the cuboidal volume, thereby invoking the servo-control algorithm, Eq. (3). During application of the confining pressure, a small amount of interparticle friction is introduced ($\phi^c=14$ deg) in order to reduce the time necessary to satisfy the convergence criterion

$$\frac{\Sigma_i-\Sigma_i^{\text{des}}}{\Sigma_i^{\text{des}}}<\beta \quad \text{with} \quad i\in\{1,2,3\} \tag{9}$$

where the tolerance β is set to 5.0×10^{-3}. Note that the convergence criterion includes all three principal stresses.

Three different confining pressures are considered, which in terms of the particle shear modulus G^{part} are: $\Sigma^{\text{conf}}/G^{\text{part}}=-2.5\times10^{-6}$, -5.0×10^{-6} and -7.5×10^{-6}. These ratios reflect a particle system that is close to the *rigid-sphere limit* ($\Sigma^{\text{conf}}/G^{\text{part}}=0$). The porosity p of the granular specimen after application of the confining pressure $\Sigma^{\text{conf}}/G^{\text{part}}=-5.0\times10^{-6}$ is 0.382. For the confining pressures $\Sigma^{\text{conf}}/G^{\text{part}}=-2.5\times10^{-6}$ and -7.5×10^{-6} the initial porosity is slightly higher and lower, respectively. The particle shear modulus and Poisson's ratio are taken as $G^{\text{part}}=20$ GPA and $\nu^{\text{part}}=0.20$, respectively. When the particle system has achieved equilibrium with the confining pressure (i.e. Eq. (9)

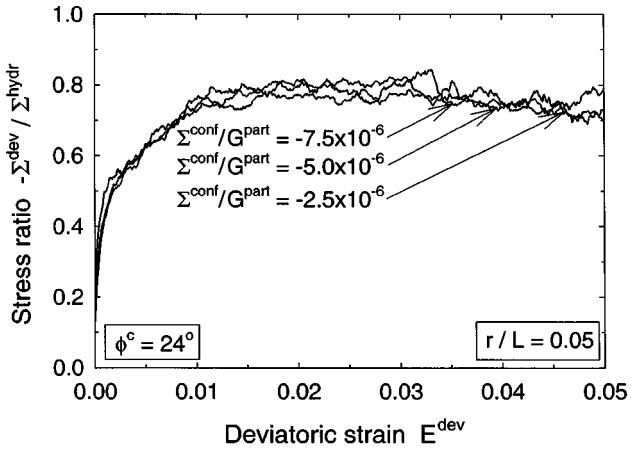

(*a*)

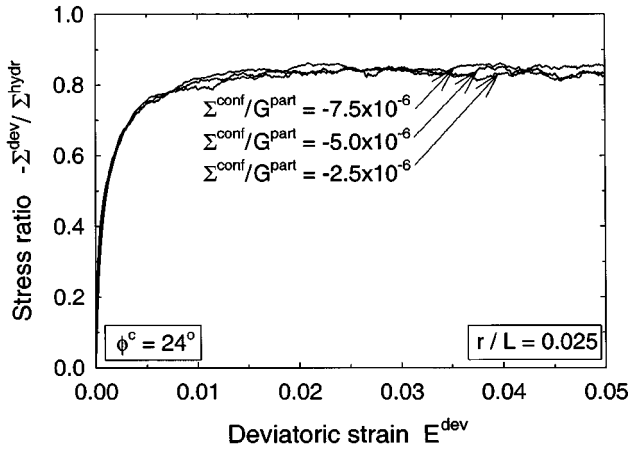

(*b*)

Fig. 2 Stress-strain response under axisymmetric compression; three confining pressures: $\Sigma^{conf}/G^{part}=-2.5\times10^{-6}$, -5.0×10^{-6} and -7.5×10^{-6} (contact friction angle $\phi^c=24$ deg). (*a*) Particle radius $r=0.05L$. (*b*) Particle radius $r=0.025L$.

is satisfied), the initial contact friction angle is incremented to the actual contact friction angle, which here equals $\phi^c=24$ deg. Subsequently, strain-controlled axial shortening is applied (in correspondence with Eq. (2)) at fixed confining pressure. Loading is terminated when the deviatoric strain has attained the value $E^{dev}=5\%$: this value is considered to be the limit of applicability of small strain theory.

In Figs. 2(*a*) and 2(*b*) the evolution of the stress ratio $-\Sigma^{dev}/\Sigma^{hydr}$ is plotted against the deviatoric strain E^{dev}, for the particle radii $r/L=0.05$ and $r/L=0.025$, respectively. The maximum stress level is reached at a deviatoric strain of approximately 2%, and shows only a mild difference in magnitude for the two cases considered. After reaching the maximum stress level, the stress remains almost constant under increasing deformation, i.e., steady-state collapse occurs. In both figures, the normalized stress-strain relations are independent of the level of confining pressure, implying that the collapse value of macroscopic deviatoric stress increases in proportion to the macroscopic hydrostatic pressure. The small differences between the individual stress-strain curves are driven by bifurcations of particle equilibrium states. If, for two granular samples, the initial characteristics at the particle level differ only slightly, (associated with different initial confining pressures), the equilibrium path to be followed will be different; this effect is more pronounced at the macroscopic level when the representative volume contains a smaller number of particles, see Figs. 2(*a*) and 2(*b*). Similar bifurcations are observed in

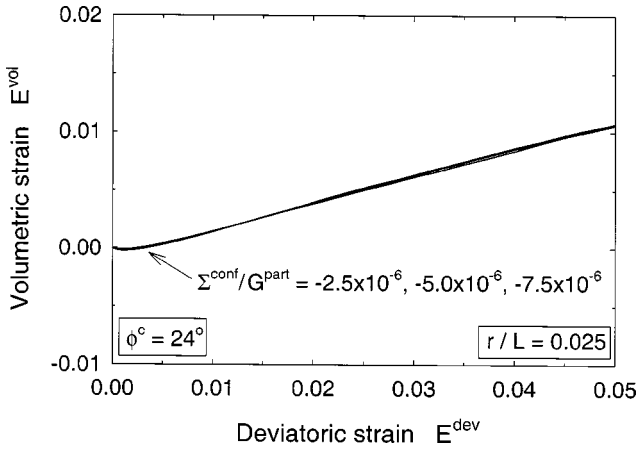

Fig. 3 Deformation characteristics under axisymmetric compression; three confining pressures: $\Sigma^{conf}/G^{part}=-2.5\times10^{-6}$, -5.0×10^{-6} and -7.5×10^{-6} (contact friction angle $\phi^c=24$ deg, particle radius $r=0.025L$)

laboratory tests on relatively coarse, noncohesive granular materials, [29], with the actual sequence of local stick-slip events between particles depending upon the initial compaction level of the material. The smoothness of the individual curves depicted in Fig. 2(*b*) indicate that the discrete system with $r/L=0.025$ responds like a continuum.

The strain response (measured after the initial confining pressure was applied) is shown in Fig. 3 for the aggregate of small particles ($r/L=0.025$). It can be seen that the response is identical for the three confining pressures considered and that proportional straining is achieved when the deviatoric strain exceeds 2%.

2.2 Influence of Contact Friction Angle Upon Macroscopic Response. The influence of the contact friction angle ϕ^c on the response is examined by simulating an axisymmetric compression test on a cuboidal volume of small particles, $r/L=0.025$. Four sets of simulations were performed, with $\phi^c=4$ deg, $\phi^c=14$ deg, $\phi^c=24$ deg, and $\phi^c=34$ deg. The specimen preparation and loading procedure are similar to those outlined in the previous section. In each simulation the confining pressure was set at $\Sigma^{conf}/G^{part}=-5.0\times10^{-6}$, corresponding to an initial porosity of $p=0.382$. Figure 4 depicts the macroscopic stress-strain curves

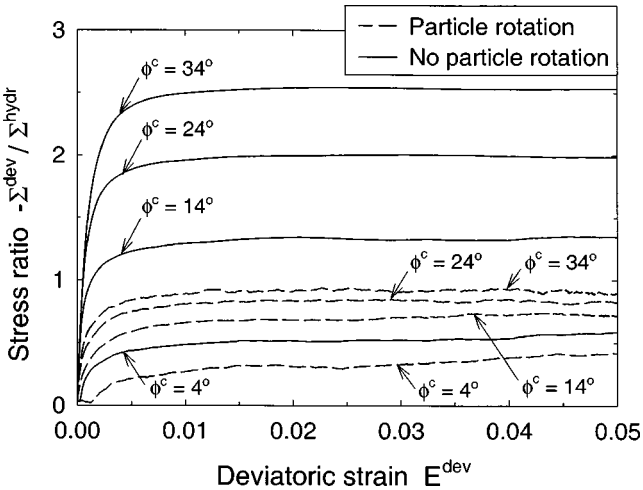

Fig. 4 Stress-strain response under axisymmetric compression; the contact friction angles are: $\phi^c=4$ deg, 14 deg, 24 deg, and 34 deg. Unconstrained and constrained particle rotation.

for the various contact friction angles considered. The ultimate collapse level increases for an increasing contact friction angle. The results of simulations with particle rotation prevented are included in the figure, and will be discussed in more detail in the subsequent section.

In order to elaborate upon the macroscopic collapse behavior, it is instructive to introduce the following set of internal state variables for the particle assembly: the *sliding contact fraction* s_f, defined by the ratio of the number of sliding contacts to the total number of contacts in the particle assembly, the *coordination number* $\bar{n}$, which is the *average* number of contacts per particle, and the *porosity* p, which equals the ratio of the void volume to the total volume occupied by the particle assembly. The steady-state values of the parameters (i.e., the values at $E^{\text{dev}}=5\%$) are plotted in Figs. 5(*a*) to 5(*c*) as a function of the contact friction angle ϕ^c. The initial value of p (after the confining pressure has been applied but with $E^{\text{dev}}=0\%$) is included in Fig. 5(*c*), and is represented by the dashed line. The plots contain results for unconstrained particle rotation and for full constraint against particle rotation; in each case the relative sliding of particles can occur in accordance with the Coulomb friction law, Eq. (1).

Consider first the sliding contact fraction s_f, as shown in Fig. 5(*a*). At steady-state collapse the number of sliding contacts decreases with increasing contact friction angle, which reflects an increase of the macroscopic strength. At the highest contact friction angle considered, $\phi^c=34$ deg, only about 10% of the total number of particle contacts is sliding, indicating that rolling of particles dominates. Both for constrained and unconstrained particle rotations the sliding contact fraction approaches zero in the limit of infinite contact friction; i.e., $s_f\rightarrow 0$ when $\phi^c\rightarrow 90$ deg. In the limit of frictionless particles, $\phi^c\rightarrow 0$ deg, the sliding contact fraction for constrained and unconstrained particle rotations should also be identical, since the deformation mechanism by particle rolling becomes inactive for particles with ideally smooth contact surfaces. The sliding contact fraction s_f is expected to approach 1.0 when $\phi^c\rightarrow 0$ deg, and the anticipated trends towards this limit have been indicated in Fig. 5(*a*) by the dashed lines. The limiting value of unity can be explained by recalling that the sliding contact fractions plotted in Fig. 5(*a*) reflect systems of nearly rigid particles that are in *neutral mechanical equilibrium* (i.e., a particle system that is on the verge of instability, as indicated in Fig. 4 by the horizontal tangential slope of the stress-strain curves at $E^{\text{dev}}=5\%$). For a system of rigid frictionless particles, a state of neutral mechanical equilibrium can be reached under isotropic loading conditions, where a network of normal contact forces is established that keeps the particle assembly just stable. When the particle system is subsequently subjected to a small deviatoric loading perturbation, all particle chains inside the contacts network will immediately collapse since the tangential resistance at every particle contact is equal to zero. Hence, all particle contacts will be subjected to sliding, and thus $s_f=1.0$. Since this collapse mechanism corresponds to zero macroscopic shear strength, it is difficult, if not impossible, to adequately simulate it by means of a discrete element analysis.

As pointed out in [30], a *minimum* average coordination number is geometrically required in order to construct a system of rigid spherical particles that is in a state of neutral equilibrium. Packing structures corresponding to a minimum average coordination number are sometimes called *isostatic packings*, [31]. For a three-dimensional isostatic packing of rigid, equi-sized *frictionless* spheres, the (minimum) coordination number is equal to 6, [30]. This value is recovered by extrapolating the curves for unconstrained and constrained particle rotation in Fig. 5(*b*) towards $\phi^c=0$ deg. For a three-dimensional isostatic packing of rigid, equi-sized *frictional* spheres which undergo no relative slip, the (minimum) coordination number is equal to 4, [32]. Again, in Fig. 5(*b*) this appears to be the asymptotic limit to which the curve for the unconstrained particle rotation decreases under increasing contact friction. In contrast, the curve for constrained particle

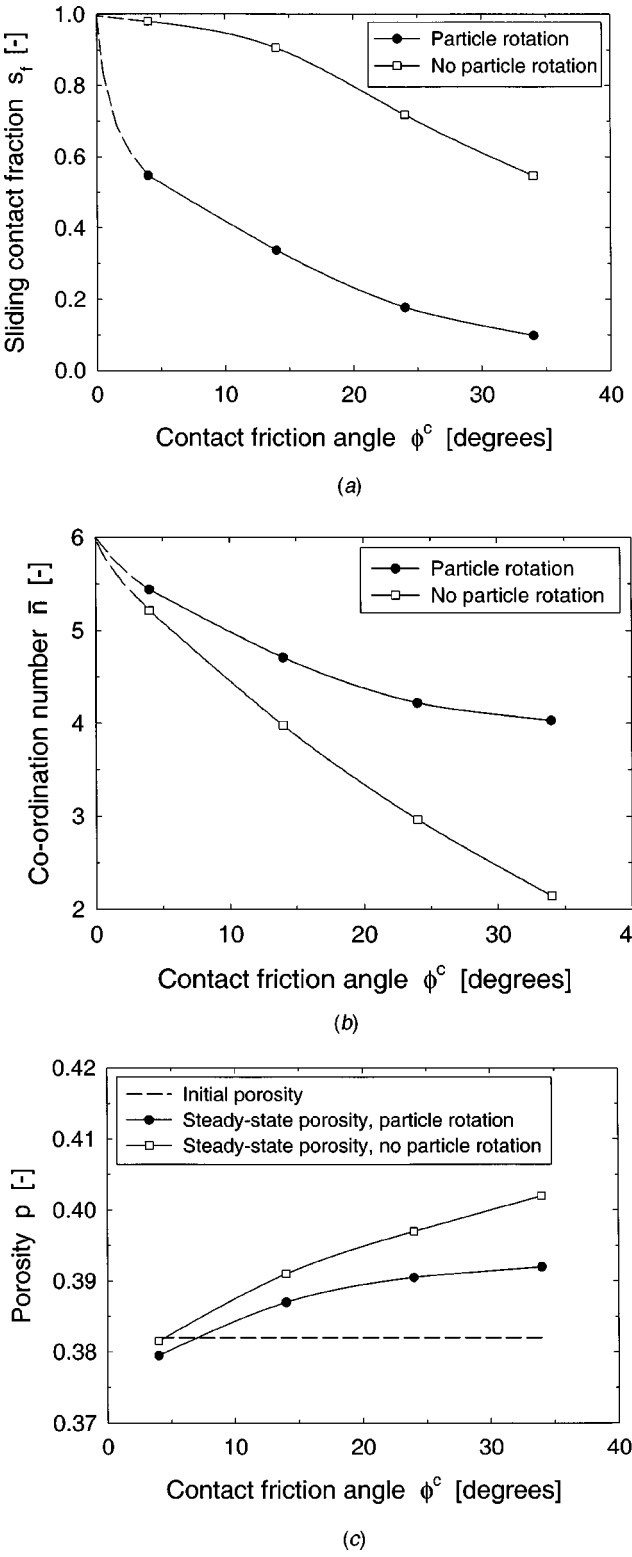

Fig. 5 Influence of contact friction angle ϕ^c on macroscopic internal state variables (for unconstrained and constrained particle rotation). (*a*) Sliding contact fraction s_f at steady-state collapse ($E^{\text{dev}}=5\%$). (*b*) Coordination number $\bar{n}$ at steady-state collapse. (*c*) Porosity p at initial state (dashed line) and at steady-state collapse (solid line).

rotation is expected to approach zero in the limit of infinite contact friction. This can be explained as follows. As discussed in [30], the minimum coordination number necessary for geometrical stability of a particle structure is directly related to the number

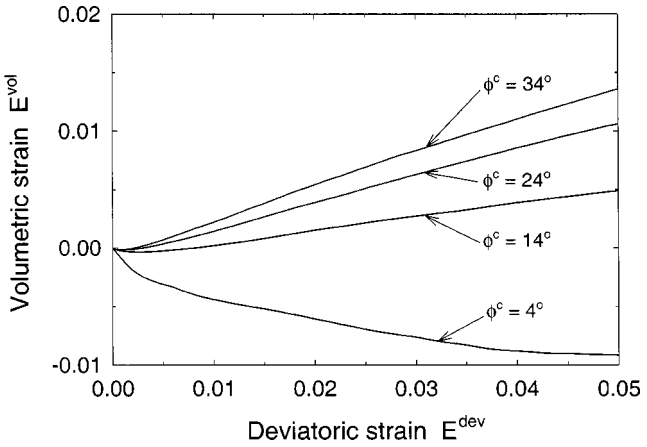

Fig. 6 Deformation characteristics under axisymmetric compression; the contact friction angles are: ϕ^c=4 deg, 14 deg, 24 deg, and 34 deg

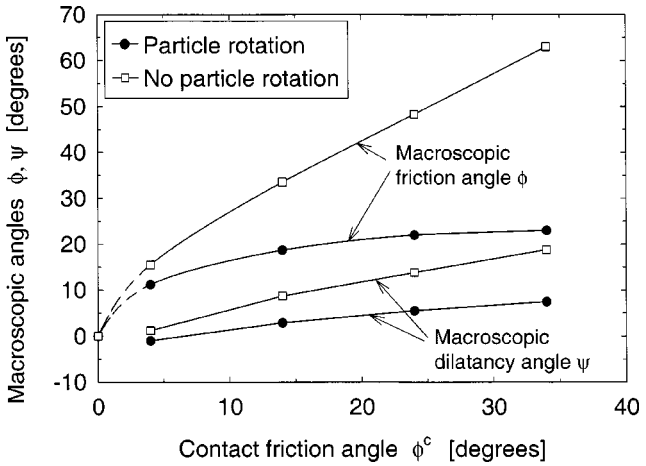

Fig. 7 Contact friction angle ϕ^c versus macroscopic friction angle ϕ and dilatancy angle ψ at steady-state collapse (E^{dev} =5%)

of internal degrees of freedom of the particle structure. An increase in contact friction leads to an increasing constraint on inter-particle sliding, whereby in the limit of infinite contact friction the internal degrees-of-freedom related to inter-particle sliding become fully constrained. The prevention of both inter-particle sliding and rolling turns the granular assembly into a rigid body with infinite shear strength and shear stiffness. Towards this limit case, the sliding contact fraction approaches zero, $s_f \rightarrow 0$; thus, most of the particles in the system will be "floating" (i.e., these particles do not transmit quasi-static forces to neighboring particles). The minimum coordination number then approaches zero because the infinite sample strength will be determined by a stable, rigid network of only a small number of contacting particles.

For the case of unconstrained particle rotation, curves with a trend similar to that in Fig. 5(*b*) were reported in [31]. Nevertheless, the particle systems of equi-sized spheres studied in [31] were obtained directly after particle deposition, which resulted in moderately stable packings with coordination numbers that are somewhat higher (between 4.5 and 6.2) than the coordination numbers for isostatic packings of rigid spheres, [30,32].

When considering the dependence of the porosity p at E^{dev} =5% upon the contact friction angle ϕ^c, see Fig. 5(*c*), it appears that p increases slightly under increasing ϕ^c. Combining this curve with the initial porosity $p=0.382$, it follows that for the lowest friction angle, $\phi^c=4$ deg, the granular assembly with unconstrained particle rotation compacts, and for greater friction angles it dilates. This is also evident from the deformation characteristics plotted in Fig. 6, where the compactive and dilative behaviors are illustrated by a monotonically decreasing volumetric strain ($\dot{E}^{vol}<0$) and a monotonically rising volumetric strain ($\dot{E}^{vol}>0$), respectively. A trend similar to that in Fig. 6 has been reported in [4] for the case of two-dimensional discrete element computations on an aggregate of circular discs under bi-axial loading. The results shown in Figs. 5 and 6 taken together have the following physical interpretation: as ϕ^c increases, the aggregate deformation at steady-state collapse becomes predominated by the rolling of particles past each other, and this results in a dilated structure with a co-ordination number approaching the minimum co-ordination number for a frictional isostatic packing.

2.3 Influence of Particle Rotation Upon Macroscopic Response. In order to explore the influence of particle rotation upon the macroscopic collapse response, the stress-strain curves for the cases where particle rotation is prevented are now compared to those where particle rotation is permitted, see Fig. 4. It can be seen that the deviatoric strength increases by a factor of two to three when particle rotation is prevented. Also, prevention of particle rotation causes steady-state collapse to be attained at a smaller strain level, and the overall response becomes smoother.

The prevention of particle rotation can be interpreted as a kinematic constraint that increases the shear strength of the granular assembly, [3,6,33]. In support of this line of reasoning, granular materials comprising angular-shaped particles (which experience restricted particle rotation due to interparticle locking) usually have a higher macroscopic shear strength at a given confining pressure than granular materials comprising round particles, [34].

Figure 7 shows the relation between the contact friction angle ϕ^c and the macroscopic friction angle ϕ, as computed by mapping the responses in Fig. 4 at E^{dev}=5% (=steady-state collapse) onto the Drucker-Prager criterion

$$F = \Sigma^{dev} + \frac{6\sin\phi}{3-\sin\phi}\Sigma^{hydr} = 0. \tag{10}$$

Under axisymmetric compression, the Drucker-Prager criterion reflects the same macroscopic friction angle as the Mohr-Coulomb hexagonal surface,

$$F = \Sigma^{hydr}\sin\phi + \frac{\sqrt{3}}{3}\Sigma^{dev}\sin\left(\theta+\frac{\pi}{3}\right) + \frac{\Sigma^{dev}}{3}\cos\left(\theta+\frac{\pi}{3}\right)\sin\phi = 0 \tag{11}$$

where θ is the angle of similarity,

$$\cos 3\theta = \frac{27}{2}\frac{J_3}{(\Sigma^{dev})^3} \quad \text{with} \quad 0 \leqslant \theta \leqslant \frac{\pi}{3}. \tag{12}$$

Here, J_3 is the third deviatoric stress invariant given by $J_3 = \Sigma'_{ik}\Sigma'_{kj}\Sigma'_{ji}/3$. Under axisymmetric compression, $\theta=\pi/3$ and Eq. (11) reduces to Eq. (10). Figure 7 clearly shows that for a higher contact friction angle the difference in macroscopic strength for unconstrained and constrained particle rotation becomes larger, indicating that the mechanism of particle rolling becomes increasingly important. As discussed in Section 2.2., the macroscopic shear strength for the assembly with constrained particle rotation is expected to become infinitely large when the contact friction approaches infinity. In contrast, for the case of unconstrained particle rotation, the macroscopic friction angle for the assembly with unconstrained particle rotation asymptotes to $\phi \approx 24°$ with increasing contact friction. In the no-sliding limit the particles are still able to roll, and therefore the macroscopic friction angle remains finite. It has already been suggested above that the macroscopic

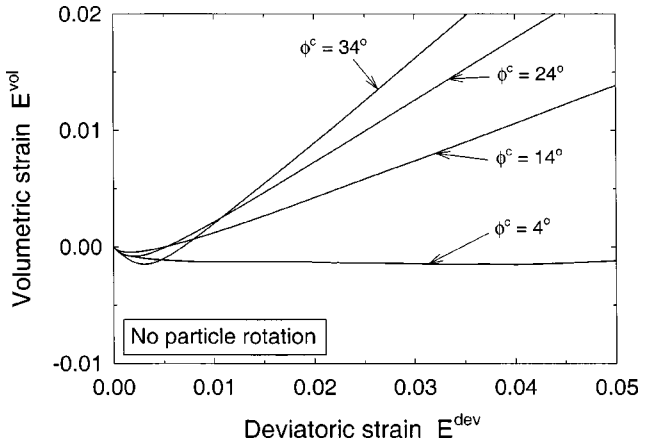

Fig. 8 Deformation characteristics under axisymmetric compression; the contact friction angles are: ϕ^c=4 deg, 14 deg, 24 deg, and 34 deg. Constrained particle rotation.

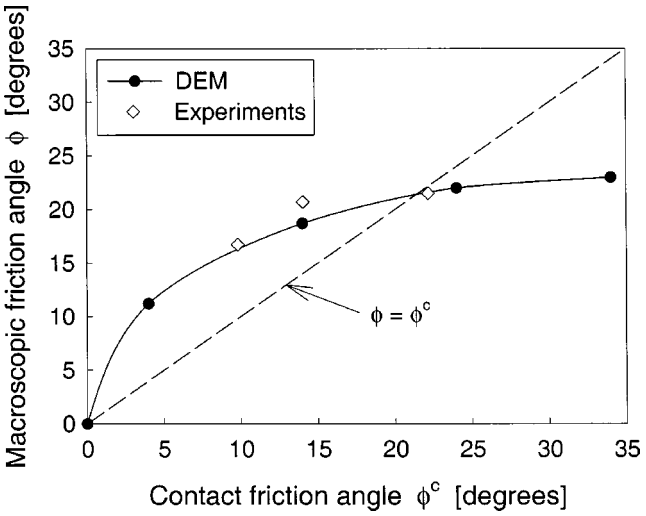

Fig. 9 Contact friction angle ϕ^c versus macroscopic friction angle ϕ. DEM versus experimental results (triaxial tests on an aggregate of steel spheres).

shear strength is zero in the limit of vanishing contact friction angle. This anticipated trend at vanishing contact friction is designated in Fig. 7 by the dashed lines.

The prevention of particle rotation also leads to an increase of the sliding contact fraction at collapse, see Fig. 5(*a*). This can be explained by the fact that prevention of particle rolling requires more particle contacts to slide in order to attain the same level of macroscopic deformation. Additionally, the prevention of particle rotation yields a lower coordination number (Fig. 5(*b*)) and a higher porosity (Fig. 5(*c*)) at steady-state collapse. Thus, the prevention of particle rotation leads to a strongly dilatant material behavior, as depicted in Fig. 8. In Figs. 6 and 8, the ratio of volumetric strain rate $\dot{E}^{\mathrm{vol}}$ to deviatoric strain rate $\dot{E}^{\mathrm{dev}}$ at $E^{\mathrm{dev}}=5\%$ defines the steady-state macroscopic dilatancy angle ψ associated with the flow potential G, where[2]

$$G=\Sigma^{\mathrm{dev}}+\frac{6\sin\psi}{3-\sin\psi}\Sigma^{\mathrm{hydr}}. \tag{13}$$

Note that the above Drucker-Prager flow potential in stress space equals the Drucker-Prager collapse criterion given by Eq. (10) when the dilatancy angle ψ is replaced by the friction angle ϕ. As usual, the direction of plastic flow is obtained by taking the stress derivative of the flow potential G. The dependence of the macroscopic dilatancy ψ upon the contact friction angle ϕ^c has been included in Fig. 7. It is clear that the macroscopic dilatancy angle is consistently less than the macroscopic friction angle, implying "nonassociated plastic flow."

2.4 Comparison of Discrete Element Simulations With Triaxial Tests on an Aggregate of Steel Spheres. A set of triaxial tests on an aggregate of steel spheres has been performed recently by Davy and Fleck (private communication) in order to explore experimentally the dependence of the steady-state macroscopic friction angle upon the contact friction angle of the spheres. A circular cylindrical sample of 50 mm diameter by 50 mm height was constructed, using spheres of approximately 4.5 mm in diameter. The aspect ratio of the granular specimen thus equals 1, and is equal to that of the discrete element model. The ratio of the sphere radius to the specimen diameter is 0.045. Although this relative particle size is somewhat bigger than that used in the discrete element simulations ($r/L=0.025$), from Figs. 2(*a*) and (*b*) it is expected that in the range $0.025<r/L<0.05$ the effect of particle size on steady-state sample strength (or steady-state macroscopic friction angle) will be very small. The sample of steel spheres was subjected to triaxial compression in three states to investigate the influence of particle contact friction: copper-coated spheres (as-received state), spheres lubricated with PTFE (polytetrafluorethylene) spray, and braze-coated spheres. The initial porosity of the samples was between 0.388 and 0.402, which is close to the initial porosity of the discrete element model (0.382). The tests involved a measurement of the steady-state macroscopic friction angle ϕ by fitting the Mohr-Coulomb collapse law, Eq. (11), to the triaxial data, and a direct measurement of the inter-particle friction between two steel spheres (which provides the contact friction angle ϕ^c). The triaxial tests follow the method described in [35], and were performed at a relatively low confining pressure (at about 0.1 MPa) in order to obtain a particle system that is close to the rigid-sphere limit.

The measured macroscopic and microscopic friction angles are plotted in Fig. 9, and are compared with the discrete element predictions where particle rotation is permitted, taken from Fig. 7. The predicted response is in excellent agreement with the experimental results. Both the discrete element method and the experiments reveal that the macroscopic friction angle ϕ exceeds the contact friction angle ϕ^c for ϕ^c less than about 21°. As ϕ^c increases, the relative proportion of inter-particle rolling to sliding increases, and ϕ levels off in value.

2.5 Influence of Particle Redistribution Upon Macroscopic Response. The effect of particle redistribution upon the macroscopic stress level can be elucidated by successively subjecting the discrete granular assembly in Fig. 1 to three different kinematic conditions: (1) particle sliding and particle rotation are allowed to occur, (2) particle sliding is allowed to occur, but particle rotation is prevented, (3) particle sliding is allowed to occur in accordance with an affine deformation field, and particle rotation is prevented. For the cases (1) and (2), the essential boundary conditions are imposed onto the outer walls of the particle assembly, see Eq. (2). In contrast, case (3) requires the translational velocity $\dot{u}_i$ of *all* particles to be prescribed, according to

$$\dot{u}_i=\dot{E}_{ij}x_j \tag{14}$$

where $\dot{E}_{ij}$ is the uniform, macroscopic strain rate and x_j are the coordinates of the particle center.

In the discrete element simulations, the contact friction angle equals $\phi^c=24$ deg, the initial confining pressure is $\Sigma^{\mathrm{conf}}=-2.5\times10^{-6}G^{\mathrm{part}}$ and the particle radius is $r=0.025L$. Two extremes of

[2]Although in the discrete element model the macroscopic strain rate is composed of elastic and permanent components, at 5% deviatoric strain the elastic strain rate is much smaller than the total strain rate. Hence, it is expected that the flow direction is not greatly in error when computed by using the values for the total strain rate.

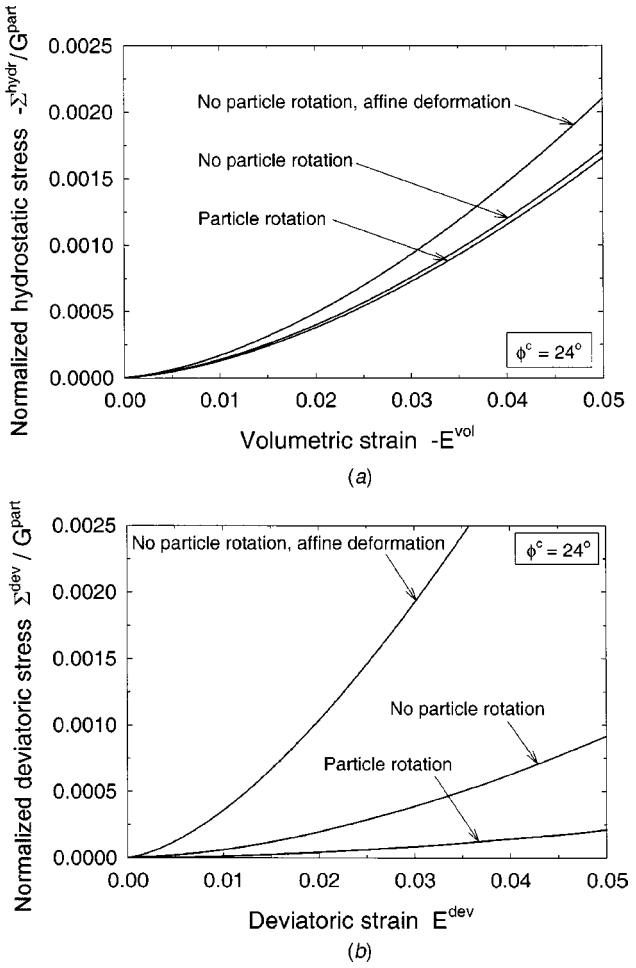

Fig. 10 Influence of particle rotation and particle rearrangement (ϕ^c=24 deg) for prescribed deformation paths. (*a*) Volumetric deformation ($\dot{E}_{11}=\dot{E}_{22}=\dot{E}_{33}$). (*b*) Deviatoric deformation ($\dot{E}_{11}=-1/2\dot{E}_{22}=-1/2\dot{E}_{33}$).

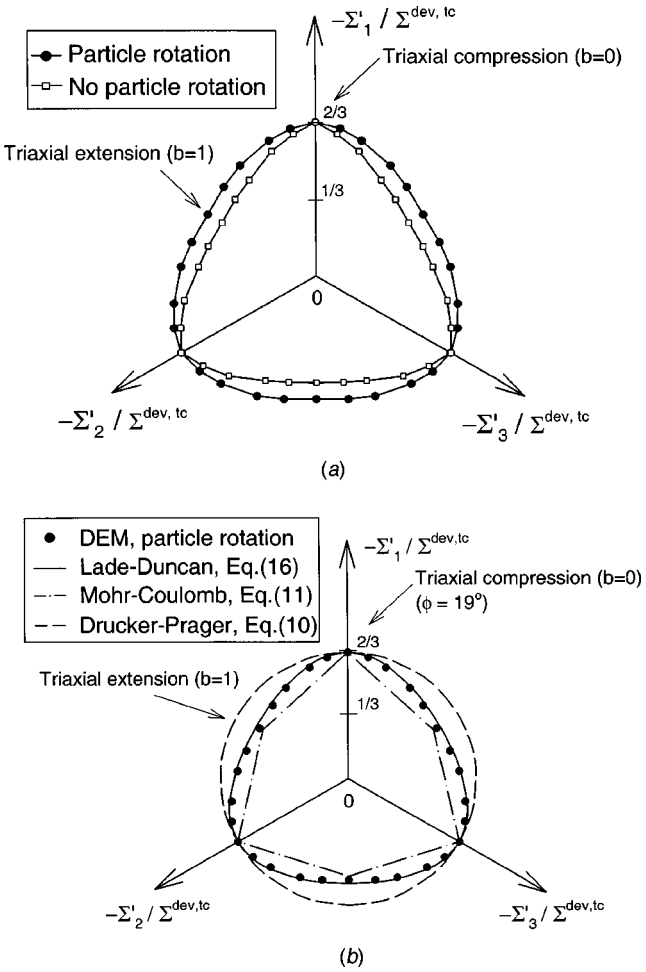

Fig. 11 Collapse contour in deviatoric plane (contact friction angle ϕ^c=24 deg). (*a*) DEM with unconstrained and constrained particle rotation. (*b*) DEM versus Lade-Duncan model, Mohr-Coulomb model and Drucker-Prager model (macroscopic friction angle ϕ=19 deg).

deformation path have been explored: *volumetric deformation*, where $\dot{E}_{11}=\dot{E}_{22}=\dot{E}_{33}$ (and $\dot{E}_{12}=\dot{E}_{23}=\dot{E}_{31}=0$) and *deviatoric deformation*, where $\dot{E}_{11}=-1/2\dot{E}_{22}=-1/2\dot{E}_{33}$ (and $\dot{E}_{12}=\dot{E}_{23}=\dot{E}_{31}=0$). For the volumetric deformation path, Fig. 10(*a*) sketches the volumetric strain versus the normalized hydrostatic stress. It is clear that the suppression of particle rotation hardly alters the macroscopic stress-strain curve. However, the introduction of an affine deformation field gives rise to noticeable stiffening. For the deviatoric deformation path, the effects of particle rotation and particle rearrangement upon the macroscopic stress level are more pronounced, see Fig. 10(*b*). The effect of particle rotation appears to strongly influence the stress magnitude, which is consistent with the result in Fig. 4. Also, the large stress increase induced by the affine deformation field suggests that substantial particle rearrangements occur when particle rotation is permitted.

For the deviatoric deformation path, at $E^{\text{dev}}=5\%$ steady-state collapse has been reached, and the macroscopic strengths are $-\Sigma^{\text{dev}}/\Sigma^{\text{hydr}}=0.94$, 1.99, and 2.74 for the cases where particle rotation is permitted, particle rotation is prevented, and affine deformation is applied, respectively. Hence, the assumption of "affine deformation," also known as the *Voigt approximation*, is not very realistic when homogenizing the mechanical behavior of an assembly of rotating particles; it would lead here to an overestimation of the macroscopic strength by a factor of 2.74/0.94=2.9.

2.6 Collapse Contour in Deviatoric Plane. The collapse contour in the deviatoric plane of the principal stress space is computed by means of *true triaxial tests*, wherein the three principal stresses depicted in Fig. 1 are varied independently. By keeping the hydrostatic pressure, Eq. (5(b)), at a constant value, a full range of radial deviatoric stress paths is imposed, as parameterized by the ratio

$$b=\frac{\Sigma_2-\Sigma_3}{\Sigma_1-\Sigma_3} \quad \text{with} \quad 0<b<1. \tag{15}$$

In Eq. (15), $b=0$ corresponds to triaxial compression (as discussed in the previous sections), while $b=1$ corresponds to triaxial extension. In the discrete element simulations, the stress-controlled loading paths, Eq. (15), are traced by invoking the servo-control algorithm, Eq. (3). Again, a cuboidal volume is randomly filled with 9167 spherical particles each of radius $r=0.025L$. The contact friction angle is assigned the value $\phi^c=24$ deg and the confining pressure equals $\Sigma^{\text{conf}}=-2.5\times10^{-6}G^{\text{part}}$.

The DEM collapse contours depicted in Fig. 11 have been composed by computing the stress states that correspond to a deviatoric strain $E^{\text{dev}}=1\%$. The axes $\Sigma_1'/\Sigma^{\text{dev},tc}$, $\Sigma_2'/\Sigma^{\text{dev},tc}$ and $\Sigma_3'/\Sigma^{\text{dev},tc}$ represent the three principal deviatoric stresses normalized by the von Mises stress under triaxial compression, $\Sigma^{\text{dev},tc}$, taken at $E^{\text{dev}}=1\%$. Figure 11(*a*) illustrates that the prevention of particle rotation provides the collapse contour with somewhat sharper corners. Further, both for constrained and unconstrained particle rotation the shear strength in triaxial compression is higher than in triaxial extension. This behavior is typical for non-

cohesive granular materials such as sand, as observed experimentally, [10,11]. In order to specify the collapse characteristics of sand in the deviatoric plane, Lade and Duncan have proposed the following phenomenological collapse criterion, [36],

$$F = I_1^3 - k_1 I_3 = 0 \tag{16}$$

where I_1, I_3 are the stress invariants

$$I_1 = 3\Sigma^{\text{hydr}} = \Sigma_{kk}$$
$$I_3 = \frac{1}{3}\Sigma_{ij}\Sigma_{jk}\Sigma_{ki} - \frac{1}{2}\Sigma_{kk}\Sigma_{ij}\Sigma_{ji} + \frac{1}{6}(\Sigma_{kk})^3 \tag{17}$$

and k_1 is a dimensionless strength parameter, which, for a cohesionless granular material, can be explicitly formulated as, [37],

$$k_1 = \frac{[\alpha(1+b)+(2-b)]^3}{b\alpha^2+(1-b)\alpha}. \tag{18}$$

In the above expression, the material parameter α is related to the macroscopic friction angle ϕ in axisymmetric compression

$$\alpha = \frac{1+\sin\phi}{1-\sin\phi} \tag{19}$$

and b characterizes the radial stress path applied, see Eq. (15). Thornton [8] has recently demonstrated close agreement between the Lade-Duncan model and a collapse contour computed by a discrete element model for a polydisperse packing of spheres (i.e., a packing of spheres with various sizes). This finding is supported by the result in Fig. 11(*b*), which depicts the collapse contour for the monodisperse packing with unconstrained particle rotation, taken from Fig. 11(*a*), together with the collapse contours of Lade-Duncan, Eq. (16), Mohr-Coulomb, Eq. (11), and Drucker-Prager, Eq. (10). It is noted that for $b=0$ Eqs. (16) and (10) are reduced to Eq. (11) for any choice of ϕ. Here, the macroscopic friction angle is prescribed as $\phi=19$ deg, in order to reproduce the DEM simulations at triaxial compression. This value is a little lower than the steady-state friction angle at triaxial compression, $\phi=22$ deg (see Fig. 7), indicating that at $E^{\text{dev}}=1\%$ the granular sample is close to steady-state collapse. As shown in Fig. 11(*b*), for stress paths other than axisymmetric compression, the Lade-Duncan model is in much better agreement with the discrete element results than the Mohr-Coulomb and Drucker-Prager models.

3 Concluding Remarks

The three-dimensional discrete element simulations discussed in this paper reveal the effect of the particle contact friction angle upon the degree of local particle rearrangement and upon the macroscopic strength. During collapse, the effect of particle rearrangement on the stress level is substantial, especially when the granular system suffers deviatoric deformations. When the collapse mechanism has reached a steady-state, the coordination number of the particle structure closely corresponds to the minimum coordination number of an isostatic packing. When the particles in the granular assembly are subjected to an affine deformation field in combination with constrained particle rotation, the mechanism of particle rearrangement is fully suppressed, leading to a considerable increase of the macroscopic stress. Accordingly, the assumption of ''affine deformation'' (the Voigt approximation), which is often adopted in the homogenization of granular materials, is far from realistic when deriving continuum models for granular assemblies with rotating particles. When only particle rotation is prevented in the discrete model, the stress level at a specific strain may still be considerably higher than for the case of unconstrained particle rotation, with the difference depending strongly on the magnitude of the particle contact friction. Preventing particle rotation also endows the collapse contour with sharper corners, implying an increase in the ratio of the shear strength under triaxial compression to the shear strength under triaxial extension.

Acknowledgments

A.S.J.S. is grateful for the hospitality offered by the Cambridge Center for Micromechanics at the Cambridge University, Cambridge, U. K., during an eight-month leave from the Delft University of Technology, Delft, The Netherlands. The authors are grateful to Dr. Catherine Davy for the provision of triaxial test data for an aggregate of steel spheres. Both authors acknowledge the EU support in the form of TMR and RTN grants ERB-4061-PL-95-0988 and HPRN-CT-2002-00198.

References

[1] Cundall, P. A., and Strack, O. D. L., 1979, ''A Discrete Numerical Model for Granular Assemblies,'' Geotechnique, **1**, pp. 47–65.
[2] Thornton, C., and Barnes, D. J., 1986, ''Computer Simulated Deformation of Compact Granular Assemblies,'' Acta Mech., **64**, pp. 45–61.
[3] Ting, J. M., Corkum, B. T., Kauffmann, C. R., and Greco, C., 1989, ''Discrete Numerical Model for Soil Mechanics,'' J. Geotech. Eng., **115**, pp. 379–398.
[4] Bathurst, R. J., and Rothenburg, L., 1990, ''Observations on Stress-Force Fabric Relationships in Idealized Granular Materials,'' Mech. Mater., **9**, pp. 65–80.
[5] Bardet, J. P., and Proubet, J., 1992, ''Shear-Band Analysis in Idealized Granular Material,'' J. Eng. Mech., **118**, pp. 397–415.
[6] Oda, M., Iwashita, K., and Kazama, H., 1997, ''Micro-Structure Developed in Shear Bands of Dense Granular Soils and Its Computer Simulation. Mechanism of Dilatancy and Failure,'' *IUTAM Symposium on Mechanics of Granular and Porous Materials*, N. A. Fleck and A. C. F. Cocks, eds., Kluwer, Dordrecht, The Netherlands, pp. 353–364.
[7] Thomas, P. A., and Bray, J. D., 1999, ''Capturing Nonspherical Shape of Granular Media With Disk Clusters,'' J. Geotech. Geoenvir. Eng., **125**, pp. 169–178.
[8] Thornton, C., 2000, ''Numerical Simulations of Deviatoric Shear Deformation of Granular Media,'' Geotechnique, **50**, pp. 43–53.
[9] Kruyt, N. P., and Rothenburg, L., 2002, ''Probability Density Functions of Contact Forces for Cohesionless Frictional Granular Materials,'' Int. J. Solids Struct., **39**, pp. 571–583.
[10] Goldscheider, M., 1976, ''Grenzbedingung und Fliessregel von Sand,'' Mech. Res. Commun., **3**, pp. 463–468.
[11] Lade, P. V., and Kim, M. K., 1988, ''Single Hardening Constitutive Model for Frictional Materials: III. Comparison With Experimental Data,'' Comput. Geotech., **6**, pp. 31–47.
[12] Christofferson, J., Mehrabadi, M. M., and Nemat-Nasser, S., 1981, ''A Micromechanical Description of Granular Material Behavior,'' ASME J. Appl. Mech., **48**, pp. 339–344.
[13] Walton, K., 1987, ''The Effective Elastic Moduli of a Random Packing of Spheres,'' J. Mech. Phys. Solids, **35**, pp. 213–226.
[14] Jenkins, J. T., 1988, ''Volume Change in Small Strain Axisymmetric Deformations of Granular Material,'' *Micromechanics of Granular Materials*, M. Satake and J. T. Jenkins, ed., Elsevier, Amsterdam, pp. 143–152.
[15] Fleck, N. A., Kuhn, L. T., and McMeeking, R. M., 1992, ''Yielding of Metal Powder Bonded by Isolated Contacts,'' J. Mech. Phys. Solids, **40**, pp. 1139–1162.
[16] Storåkers, B., Fleck, N. A., and McMeeking, R. M., 1999, ''The Viscoplastic Compaction of Composite Powders,'' J. Mech. Phys. Solids, **47**, pp. 785–815.
[17] Liao, C. L., Chan, T. C., Suiker, A. S. J., and Chang, C. S., 2000, ''Pressure-Dependent Elastic Moduli of Granular Assemblies,'' Int. J. Numer. Analyt. Meth. Geomech., **24**, pp. 265–279.
[18] Suiker, A. S. J., de Borst, R., and Chang, C. S., 2001, ''Micro-Mechanical Modelling of Granular Material—Part 1: Derivation of a Second-Gradient Micro-Polar Constitutive Theory,'' Acta Mech., **149**, pp. 161–180.
[19] Suiker, A. S. J., de Borst, R., and Chang, C. S., 2001, ''Micro-Mechanical Modelling of Granular Material—Part 2: Plane Wave Propagation in Infinite Media,'' Acta Mech., **149**, pp. 181–200.
[20] Digby, P. J., 1981, ''The Effective Elastic Moduli of Porous Granular Rock,'' ASME J. Appl. Mech., **48**, pp. 803–808.
[21] Chang, C. S., Sundaram, S. S., and Misra, A., 1989, ''Initial Moduli of Particulated Mass With Frictional Contacts,'' Int. J. Numer. Analyt. Meth. Geomech., **13**, pp. 629–644.
[22] Liao, C. L., Chang, T. P., Young, D. H., and Chang, C. S., 1997, ''Stress-Strain Relationships for Granular Materials Based on the Hypothesis of Best-Fit,'' Int. J. Solids Struct., **34**, pp. 4087–4100.
[23] Heyliger, P. R., and McMeeking, R. M., 2001, ''Cold Plastic Compaction of Powders by a Network Model,'' J. Mech. Phys. Solids, **49**, pp. 2031–2054.
[24] Redanz, P., and Fleck, N. A., 2001, ''The Compaction of a Random Distribution of Metal Cylinders by the Discrete Element Method,'' Acta Mater., **49**, pp. 4325–4335.
[25] Johnson, K. L., 1985, *Contact Mechanics*, Cambridge University Press, London, UK.
[26] Cundall, P. A., 1988, ''Computer Simulations of Dense Sphere Assemblies,'' *Micromechanics of Granular Materials*, M. Satake and J. T. Jenkins, ed., Elsevier, Amsterdam, pp. 113–123.
[27] Bathurst, R. J., and Rothenburg, L., 1988, ''Micromechanical Aspects of Isotropic Granular Assemblies With Linear Contact Interactions,'' ASME J. Appl. Mech., **55**, pp. 17–23.

[28] Torquato, S., 2002, *Random Heterogeneous Materials, Microstructure and Macroscopic Properties*, Springer-Verlag, New York.
[29] Suiker, A. S. J., 2002, *The Mechanical Behavior of Ballasted Railway Tracks*, dissertation, Delft University Press, Delft, The Netherlands (pdf-format available at http://www.library.tudelft.nl/dissertations/).
[30] Alexander, S., 1998, ''Amorphous Solids: Their Structure, Lattice Dynamics and Elasticity,'' Phys. Rep., **296**, pp. 65–236.
[31] Silbert, L. E., Ertaş, D., Grest, G. S., Halsey, T. C., and Levine, D., 2002, ''Geometry of Frictionless and Frictional Sphere Packings,'' Phys. Rev. E, **65**(031304), pp. 1–6.
[32] Edwards, S. F., 1998, ''The Equations of Stress in a Granular Material,'' Physica A, **249**, pp. 226–231.
[33] Ng, T. T., and Dobry, R., 1994, ''A Non-linear Numerical Model for Soil Mechanics,'' J. Geotech. Eng., **120**, pp. 388–403.
[34] Lambe, T. W., and Whitman, R. V., 1969, *Soil Mechanics*, John Wiley and Sons, New York.
[35] Davy, C. A., Fleck, N. A., and Bolton, M. D., 2004, ''The Collapse Behavior of a Sugar Aggregate,'' submitted, for publication.
[36] Lade, P. V., and Duncan, J. M., 1975, ''Elastoplastic Stress-Strain Theory for Cohesionless Soil,'' J. Geotech. Eng., **101**, pp. 1037–1053.
[37] Chen, W. F., and Saleeb, A. F., 1982, *Constitutive Equations for Engineering Materials*, John Wiley and Sons, New York.